Monthly Notices of the ROYAL ASTRONOMICAL SOCIETY

MNRAS **458,** 708–717 (2016) doi:10.1093/mnras/stw175

Are the distributions of fast radio burst properties consistent with a cosmological population?

M. Caleb,[1,2,3★] C. Flynn,[2,3] M. Bailes,[2,3] E. D. Barr,[2,3] R. W. Hunstead,[4] E. F. Keane,[5,2,3] V. Ravi[2] and W. van Straten[2]

[1]*Research School of Astronomy and Astrophysics, Australian National University, ACT 2611, Australia*
[2]*Centre for Astrophysics and Supercomputing, Swinburne University of Technology, PO Box 218, Hawthorn, VIC 3122, Australia*
[3]*ARC Centre of Excellence of All-sky Astrophysics (CAASTRO)*
[4]*Sydney Institute for Astronomy (SIfA), School of Physics, The University of Sydney, NSW 2006, Australia*
[5]*SKA Organization, Jodrell Bank Observatory, Cheshire SK11 9DL, UK*

Accepted 2016 January 19. Received 2016 January 3; in original form 2015 September 7

ABSTRACT

High time resolution radio surveys over the last few years have discovered a population of millisecond-duration transient bursts called fast radio bursts (FRBs), which remain of unknown origin. FRBs exhibit dispersion consistent with propagation through a cold plasma and dispersion measures indicative of an origin at cosmological distances. In this paper, we perform Monte Carlo simulations of a cosmological population of FRBs, based on assumptions consistent with observations of their energy distribution, their spatial density as a function of redshift and the properties of the interstellar and intergalactic media. We examine whether the dispersion measures, fluences, derived redshifts, signal-to-noise ratios and effective widths of known FRBs are consistent with a cosmological population. Statistical analyses indicate that at least 50 events at Parkes are required to distinguish between a constant comoving FRB density, and an FRB density that evolves with redshift like the cosmological star formation rate density.

Key words: methods: data analysis – surveys – pulsars: general – cosmology: miscellaneous.

1 INTRODUCTION

Fast radio bursts (FRBs) are bright (few Jy), radio pulses occurring with time-scales of the order of milliseconds. 18 bursts have been discovered to date (Lorimer et al. 2007; Thornton et al. 2013; Burke-Spolaor & Bannister 2014; Spitler et al. 2014; Champion et al. 2015; Masui et al. 2015; Petroff et al. 2015a; Ravi, Shannon & Jameson 2015; Keane et al. in preparation; Ravi et al. in preparation) The integrated electron densities along the lines of sight to these bursts (called dispersion measures, or DMs) lie in the range of 375–1600 pc cm^{-3}. This is greatly in excess of the expected contribution from the Galaxy via the interstellar medium (ISM; Cordes & Lazio 2002) along such lines of sight, which typically lie in the range of 20–50 pc cm^{-3}.

For all FRBs discovered to date, the arrival time delay associated with the dispersion closely follows a ν^{-2} frequency dependence, and the pulse width evolution follows a ν^{-4} frequency dependence for those FRBs where the signal-to-noise ratio (S/N) has permitted frequency-dependent width measurements (Thornton et al. 2013). Both properties are consistent with propagation through a sparse, non-relativistic plasma.

A few years after the publication of the first FRB (Lorimer et al. 2007) another population of sources (dubbed Perytons) was identified at the Parkes 64 m radio telescope that were clearly not of extraterrestrial origin. The Perytons (Burke-Spolaor et al. 2011) also show swept-frequency properties, although they tend to be broader, mimic interstellar scattering and typically occur during meal-times on-site. Unlike the FRBs, the Perytons appeared in all 13 beams of the Parkes multibeam (MB) receiver, indicative of a terrestrial origin. The Perytons were ultimately shown to be originating from improperly shielded microwave ovens (Petroff et al. 2015b).

Given their large DMs, Lorimer et al. (2007) and Thornton et al. (2013) have proposed that FRBs lie at cosmological distances, and that their DMs are dominated by propagation through the intergalactic medium (IGM), with minor contributions from the ISM in the Milky Way and the ISM in a putative host galaxy. Redshift estimates to the sources are made by subtracting the ISM component of the DM, and ascribing the rest to propagation through the IGM for which the electron density is available from cosmological models. For the 15 published FRBs, the redshift estimates are in the range $0.2 < z < 1.5$, firmly placing the sources at cosmological distances. As the IGM is thought to contain 90 per cent of the Universe's baryons,

★ E-mail: manisha.caleb@anu.edu.au

(e.g. Fukugita & Peebles 2004; Savage et al. 2014), measuring the DMs of FRBs at high redshifts is potentially a novel way to probe this important cosmological component. Furthermore, if placed at such distances, the unbeamed (isotropic) energies of the observed FRBs lie in the range 10^{31}–10^{33} J (Keane & Petroff 2015). The observed FRBs also have brightness temperatures well in excess of thermal emission ($T_b > 10^{33}$ K), strongly suggesting coherent emission (Katz 2014; Luan & Goldreich 2014).

Four events were found by Thornton et al. (2013) in the high-latitude component of the High Time Resolution Universe (HTRU) survey at Parkes (Keith et al. 2010). From these events, a rate of $\gtrsim 1.0^{+0.6}_{-0.5} \times 10^4$ events sky^{-1} d^{-1} was estimated. If the redshifts ascribed to the bursts are valid, the volumetric rate to which this corresponds is $\sim 2 \times 10^4$ events Gpc^{-3} yr^{-1}, which is similar to the volumetric rate for soft gamma-ray repeaters (SGRs) ($<2.5 \times 10^4$ events Gpc^{-3} yr^{-1}), and within an order of magnitude of the volumetric rate of core-collapse (Type II) supernovae ($\sim 2 \times 10^5$ events Gpc^{-3} yr^{-1}; Kulkarni et al. 2014).

A cosmological origin for the excess DM of FRBs is not the only possibility, as FRBs could be Galactic objects in high electron density environments which electron density models for the Milky Way do not capture. This has been discussed by (Loeb, Shvartzvald & Maoz 2014), who propose FRBs originate from low-mass main-sequence 'flare stars'. No consensus has emerged regarding the progenitors of FRBs no matter whether Galactic or extra-Galactic, with possibilities including flare stars (Loeb et al. 2014, Galactic) and extra-Galactic sources such as annihilating black holes (Keane et al. 2012), giant flares from SGRs (Popov & Postnov 2013; Thornton et al. 2013; Lyubarsky 2014), binary white dwarf mergers (Kashiyama, Ioka & Mesaros 2013), neutron star mergers (Totani 2013), collapsing supramassive neutron stars (Falcke & Rezzolla 2014), radio emission from pulsar companions (Mottez & Zarka 2014), dark matter induced collapse of neutron stars (Fuller & Ott 2015) and the radio emission from pulsars (Connor, Sievers & Pen 2015; Cordes & Wasserman 2016). In this paper, we concentrate explicitly on an extra-Galactic origin for FRBs.

We present here simulations of a cosmological population of FRBs, under assumptions about their energy distribution, their spatial density as a function of redshift and the properties of the ISM and IGM (Section 2), finding they are broadly consistent with origin at cosmological distances. The analysis of the models and the results are discussed in Section 3, in comparison with data from the HTRU survey. We present log$N$–log$\mathcal{F}$ curves and discuss the FRB rates at Parkes and UTMOST in Section 4 and finally our summary and conclusions in Section 5.

2 MONTE CARLO SIMULATIONS

The HTRU survey at Parkes samples the transient radio sky with 64 μs resolution at 1352 MHz and has a bandwidth of 340 MHz. The observing band is sub-divided into 390.625 kHz frequency channels. HTRU is composed of three sub-surveys at low, intermediate and high Galactic latitudes. The simulations in this paper are of the high-latitude (Hilat) region of the survey – 34099, 270 s pointings at declinations $\delta < 10^\circ$ – where nine of the 18 known FRBs have been discovered (Thornton et al. 2013; Champion et al. 2015), and of the intermediate latitude (Medlat) region, which yielded no FRBs (Petroff et al. 2014). Petroff et al. (2014) and Hassall, Keane & Fender (2013) have carried out studies similar to ours, to model the detectability of FRBs using simulations and analytic methods, respectively. Petroff et al. (2014) simulated the effects of dispersion smearing which is the pulse broadening caused by the adopted frequency resolution, interstellar scattering and sky temperature on FRB sensitivity at Parkes, in the Medlat region. Hassall et al. (2013) used analytical methods to derive the detection rates at various telescopes operating over a wide range of frequencies. Our simulations are of FRB events at cosmological distances under assumptions about their comoving density with redshift, and include the effects of ISM scattering, IGM scattering, dispersion smearing, sky temperature and telescope beam pattern. We produce estimates of the energy, fluence, S/N, pulse width, DM and redshift distributions for FRBs with our models, and compare them to the nine FRBs detected in Hilat. We perform two classes of simulations:

(i) in Section 2, we generate numerous events such that the Poisson noise of the simulations in Figs 1 and 2 is negligible compared to the noise of the nine Hilat events,

(ii) in Section 3.4, we generate thousands of short runs with an average of nine events per simulation to estimate and compare the slopes of their log$N$–log$\mathcal{F}$ curves with the slope of the log$N$–log$\mathcal{F}$ curve of the nine Hilat FRBs.

For simplicity, FRB events in our simulations are assumed to be radiating isotropically at the source with a flat spectrum to be consistent with what is seen at 20 cm with Parkes. Their intrinsic energy distribution is assumed to be lognormal. We adopt a ΛCDM model with matter density $\Omega_m = 0.27$, vacuum density $\Omega_\Lambda = 0.73$ and Hubble constant $H_0 = 71$ km s^{-1}Mpc^{-1} (Wright 2006). The comoving number density distribution of FRBs in the simulations is assumed to be either a constant, or proportional to the cosmic star formation history (SFH). We adopt the SFH from the review paper of Hopkins & Beacom (2006) as typical of cosmic SFH measurements, which show a rise in the star formation rate (SFR) of about an order of magnitude between the present ($z = 0$) and redshifts of $z \sim 2$ (see their fig. 1). It has the parametric form $\dot{\rho}_* = (a + bz)h/[1 + (z/c)^d]$ where $h = 0.7$, $a = 0.0170$, $b = 0.13$, $c = 3.3$ and $d = 5.3$ (see their section 4). We do not explicitly set the comoving number density of FRBs in the simulation: we compute the maximum in the product of SFH and comoving volume of each shell of width dz as a function of z, and generate Monte Carlo events under this function. This allows the simulation to generate events at the maximum rate, which is important as our run times can be quite long (cf. Section 3).

The total DM for any given FRB is assumed to arise from a component due to the IGM, a component due to the ISM in a putative host galaxy and a component due to the ISM of the Milky Way:

$$\mathrm{DM_{tot}} = \mathrm{DM_{IGM}} + \mathrm{DM_{ISM}} + \mathrm{DM_{host}}. \quad (1)$$

These different DM components are modelled as follows.

(i) The DM due to the IGM is assumed to be related to the redshift of the source via the simple scaling relation $\mathrm{DM_{IGM}} = 1200\, z$ pc cm^{-3} with a 1σ scatter of the order of $\sim$20 per cent over the redshift range and DM range of interest (DM>100, $0.5 \lesssim z \lesssim 2$; Ioka 2003; Inoue 2004).

(ii) The contribution due to the ISM of the Milky Way along the line of sight to each event is taken from the NE2001 model of Cordes & Lazio (2002) which includes the electron density distributions in the thin disc, thick disc, spiral arms and Galactic Center components. For the high Galactic latitude regions simulated, this is generally, $\lesssim$50 pc cm^{-3}.

(iii) The DM contribution of a putative host galaxy will depend on galaxy type, the FRB site within it and the viewing angle. Xu & Han (2015) have modelled the DM distributions due to the ISM for

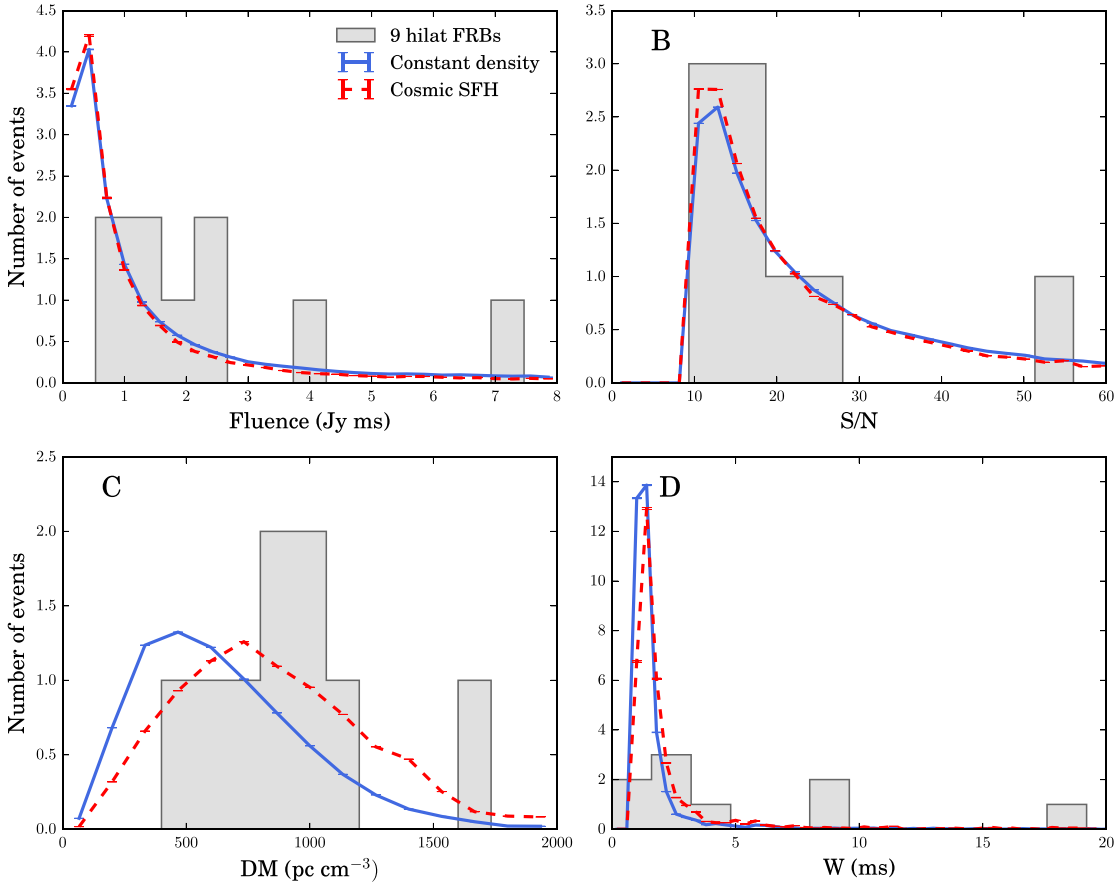

Figure 1. Simulated and observed distributions of fluence, S/N, DM and width for the nine Parkes events. The dashed and solid curves represent the cosmic SFH and constant comoving density, respectively. The nine observed FRB events are represented by the histograms. The values of the data have been obtained using the HEIMDALL (http://sourceforge.net/projects/heimdall-astro/) single pulse detection software package. Panel A: fluence distribution predicted by both models. Panel B: S/N distribution above the detection threshold of the FRBs. Panel C: FRB distribution as a function of total DM. Panel D: the observed widths distribution predicted by both models.

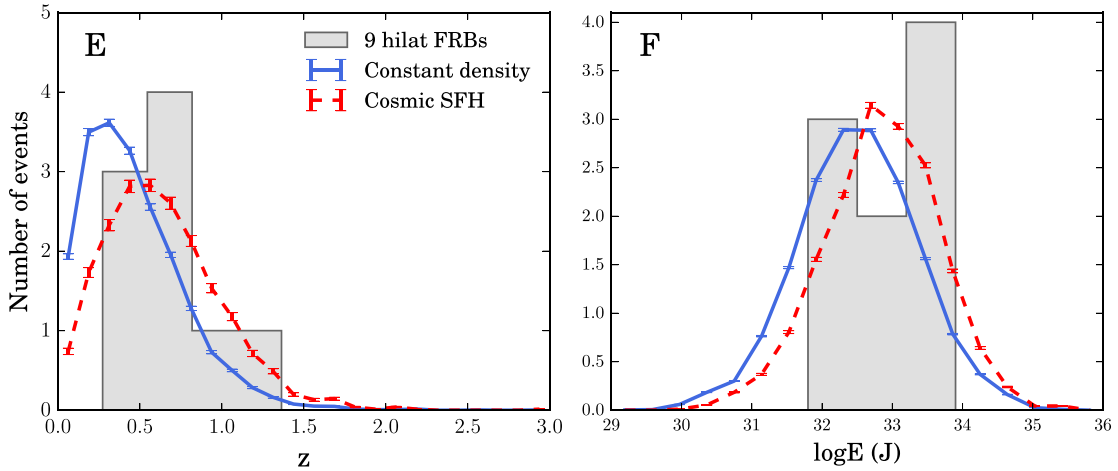

Figure 2. Derived FRB parameters from the Monte Carlo simulations of FRBs detected in the Hilat survey at Parkes. The dashed and solid curves represent the cosmic SFH and constant comoving density models for the FRB spatial densities, respectively. The nine observed Parkes FRB events are represented by the histograms. Panel E: FRB distribution as a function of redshift. Panel F: unbeamed energy distribution of the FRBs.

FRBs arising in elliptical, dwarf and spiral galaxies. They scale the NE2001 model of the Milky Way ISM to the integrated Hα intensity maps for such hosts, to represent their electron density distributions. The ensemble average DM distribution for dwarf galaxies is 45 pc cm^{-3} and for elliptical galaxies is 37 pc cm^{-3}. For spirals, they derive the weighted average of the DM distribution over a range of inclination angles ($0^\circ, 30^\circ, 60^\circ, 75^\circ, 90^\circ$) to be 142 pc cm^{-3}. Noting that there may be more than one type of FRB progenitor Masui et al. (2015) conclude that their particular FRB could have occurred in a high density or star-forming region of a host galaxy due to

Table 1. Specifications of Parkes MB, Parkes PAF and UTMOST.

Parameter	Unit	Parkes MB (Keith et al. 2010)	Parkes PAF[a]	UTMOST[b] (Bailes et al. in preparation)
Field of view	$\deg^2$	0.55	2.2	4.64×2.14
Central beam gain	K Jy^{-1}	0.7	0.9	3.5
Central beam T_{sys}	K	21	50	70
Bandwidth	MHz	340	340	16
Frequency	MHz	1352	1352	843
Channel width	MHz	0.390 625	∼1	0.781 25
No. of polarizations	–	2	2	1
Polarization feeds	–	Dual linear	Dual linear	Right circular

[a]http://www.atnf.csiro.au/management/atuc/2013dec/science_meeting/ATUC_PKS_receivers.pdf
[b]UTMOST's full Bandwidth is 31.25 MHz.

its high linear polarization. Observationally, the galaxy stellar mass function distribution peaks near the Milky Way mass (Robles et al. 2008, their fig. 9), and we assume that the DM properties of the Milky Way are typical of a host FRB galaxy. Probing many random lines of sight through the NE2001 model, we derive a median DM of $\sim$70pc cm^{-3} for the Milky Way. Given the wide range of DM estimates above, and the uncertainty even as to what typical host galaxies are and the sites of FRBs within them, we have decided to follow Thornton et al. (2013) and Xu & Han (2015), and assume a DM value of $DM_{host} \sim 100$ pc cm^{-3} as typical over a range of hosts and inclination angles. This assumption is somewhat ad hoc, but does have the advantage of facilitating comparison with previous work. The assumed DM of the host is a small fraction of the total DM to FRBs both in our observed samples and in the simulations, and we could vary this host galaxy DM over the full range discussed above ($40 \lesssim$ DM $\lesssim 140$) and not affect the conclusions of the paper.

In the simulation, events are generated out to a redshift $z = 3.0$ in shells of width $dz = 0.01$, each populated in proportion to the comoving volume of the shell and weighted by the SFR at its redshift z (in 'SFH' type models). Events are distributed randomly over the sky surveyed by Hilat in proportion to the total time spent on sky (i.e. the product of the number of pointings and the integration time per pointing). No events are generated north of declination $\delta = +10^\circ$, the northern limit of the survey performed at Parkes.

The fluence $\mathcal{F}$ (in Jy ms) at the telescope is derived from the energy at the source E, the luminosity distance in the ΛCDM cosmology and a factor of $(1 + z)$ representing the redshifting of the observed frequency range, given by

$$\mathcal{F} = \frac{10^{29}\, E}{4\pi {D_{\rm L}}^2(z)\, B\, (1+z)} \ {\rm Jy\,ms}, \tag{2}$$

where z is the redshift; $D_{\rm L}(z)$ is the luminosity distance in pc; E is isotropic emitted energy in J; B is the bandwidth of the receiver system in Hz. The S/N of each event is determined using the radiometer equation,

$$\mathrm{S/N} = \beta\, \frac{S\, G\, \sqrt{B\, t\, N_{\rm p}}}{T_{\rm rec} + T_{\rm sky}}, \tag{3}$$

where S is the flux of the signal in Jy, β is the digitisation factor $\simeq$ 1.0, B is the bandwidth in Hz, $N_{\rm p}$ is the number of polarizations, t is the pulse width in seconds, $T_{\rm rec}$ and $T_{\rm sky}$ are the receiver and sky temperatures in K, respectively, and G is the system gain in K Jy^{-1}.

Additional simulations of the FRB rates in other surveys are made later in the paper, and the parameters adopted in those simulations are shown in Table 1.

The brightest FRB in Thornton et al. (2013), namely FRB110220 was detected with S/N of $\sim$ 50 and has an estimated energy $E = 10^{32.5}$ J at source, a pulse width of $W = 5.6$ ms, redshift of $z = 0.81$ and a luminosity distance of $D_{\rm L}(z) = 5.1$ Gpc. Thornton et al. (2013) assumed the FRBs were radiating into 1 sr (that is with a beaming fraction of $1/4\pi$), whereas we assume isotropic radiation instead for simplicity. Accounting for this factor means that the isotropic energy of FRB110220 in the rest frame is $E = 10^{33.6}$ J and its fluence is 7.3 Jy ms.

2.1 Scattering

Along the path from source to receiver, a radio pulse may be broadened in several ways. We assume the scatter-broadening time (τ) of a pulsed signal passing through the ISM is related to the DM by the empirical function derived by Bhat et al. (2004):

$$\log(\tau_{\rm ISM}) = -6.5 + 0.15\log({\rm DM_{ISM}} + 1.1\log({\rm DM_{ISM}})^2 - 3.9\log\nu, \tag{4}$$

where $\tau_{\rm ISM}$ is in ms and ν is in GHz. Rescaling the scatter-broadening time through the ISM for the IGM, Lorimer et al. (2013) arrived at an upper limit to the average amount of scattering as a function of DM, with the scattering due to the IGM being three orders of magnitude smaller than that due to the ISM, i.e.

$$\log(\tau_{\rm IGM}) = \log(\tau_{\rm ISM}) - 3.0. \tag{5}$$

This rescaling on scattering in the IGM is still consistent with the observed widths of the majority of the FRBs discovered to date (Lorimer et al. 2013).

Additionally, the pulse is broadened or smeared across frequency channels because of the adopted frequency resolution $\tau_{\rm DM} = 8.3\,\Delta\nu\,{\rm DM}\,\nu^{-3}\,(\mu{\rm s})$, where DM is in pc cm^{-3}, $\Delta\nu$ is the channel bandwidth in MHz and ν is in GHz. The observed width W of the FRB taking into account the different contributing components is

$$W^2 = \tau_{\rm IGM}^2 + \tau_{\rm ISM}^2 + \tau_{\rm int}^2 + \tau_{\rm DM}^2 + \tau_{\delta\rm DM}^2 + \tau_{\rm samp}^2 + \tau_{\delta\nu}^2, \tag{6}$$

where the first two components are the scattering times due to the IGM and ISM, $\tau_{\rm int}$ is the (unknown) intrinsic width of the pulse, $\tau_{\rm DM}$ is due to the DM smearing, $\tau_{\delta\rm DM}$ is the second-order correction to the DM smearing, $\tau_{\rm samp}$ is due to the adopted sampling time and $\tau_{\delta\nu}$ is the filter response of an individual frequency channel (Cordes & McLaughlin 2003). The $\tau_{\delta\rm DM}$ and $\tau_{\delta\nu}$ terms are typically negligible in the context of our modelling. For the FRBs discovered at Parkes to date, $\tau_{\rm IGM}$ ranges from $\sim$2 μs to $\sim$40 ms and $\tau_{\rm ISM}$ ranges from $\sim$40 ns to $\sim$10 ms. Previous studies dealing with FRB detectability have assumed either a 'no scattering' scenario or a strong ISM-like scattering scenario for the IGM, as its properties are highly

uncertain. Macquart & Koay (2013) have suggested that if the latter scenario was true, the FRB pulses will be rendered undetectable at current telescopes, concluding that the IGM scattering was likely weak ($\leq$1 ms). We may therefore be sampling a highly selected population of FRBs, both in terms of luminosity and scattering.

The total width of a simulated event W affects its S/N ratio, scaling it down by a factor proportional to $\sqrt{W}$. This essentially limits the horizon of the HTRU survey to $z \sim 2$ as dispersive effects beyond this redshift rapidly degrade the S/N of even the brightest events to well below the adopted threshold of 10. Consequently, we use $z = 3.0$ as the high redshift cut-off in the simulations. This is sufficiently far to sample the DM space of the known FRBs.

2.2 Measured signal-to-noise ratios

The sky temperature additionally degrades the S/N particularly for sources close to the Galactic plane. We adopt a receiver temperature[1] of $T_{\rm rec} = 21$ K at Parkes and estimate the sky temperature ($T_{\rm sky}$) at the Galactic longitude and latitude (l, b) of the source from Haslam et al. (1982) who mapped the sky temperature at 408 MHz with a resolution of $0.^{\circ}85 \times 0.^{\circ}85$. We scaled the survey frequency of 408 MHz to the HTRU frequency of 1.4 GHz by adopting a spectral index of -2.6 for the Galactic emission (Reich & Reich 1988), i.e.

$$T_{\rm sky} = T_{\rm sky_{(l,b)}} \left(\frac{\nu}{408.0\,{\rm MHz}} \right)^{-2.6}. \quad (7)$$

The S/N of each FRB event is then reduced by the additional factor $T_{\rm rec}/(T_{\rm rec} + T_{\rm sky})$. For most sources this is a negligible correction, becoming important only near the Galactic Centre and low in the Galactic plane. $T_{\rm sky}$ at high latitudes is typically $\sim$1 K and lies between 3 and 30 K over the Medlat regions.

The S/N is finally degraded depending on a randomly chosen position in the beam pattern. For Parkes, each beam of the MB receiver is represented as an Airy disc with a 14.4 arcmin full-width half-maximum. It should be noted that the effect of the beam pattern is quite significant on the distribution of both the event S/N and the apparent luminosity; this is discussed in detail in Section 3.3.

3 ANALYSIS AND RESULTS

We have simulated FRBs in two models for their comoving number density (either following the SFH, or simply constant density) and either including or excluding the effects of scattering. In each model, we adopt a lognormal source luminosity distribution, centred on a mean energy E_0 and spread $\sigma_{\rm logE}$. The average energy of the four Thornton et al. (2013) events in Keane & Petroff (2015) correcting for the beaming fraction is $10^{32.8}$ J. We initially adopt $\log E_0 = 32.8$ and a spread of $\sigma_{\rm logE} = 1.0$, as this is the order of magnitude scatter seen on the Thornton et al. (2013) events. Within a given model choice for the source density with redshift, E_0 and $\sigma_{\rm logE}$ are the two free parameters.

The simulations were run on 12 CPU cores with run times of a few days on the gSTAR national facility at the Swinburne University of Technology. Millions of FRBs are typically generated in the runs, the vast majority of which are too dim to see. We ran the simulations until we had $\sim$5000 FRBs that passed the selection criteria, to ensure good statistical sampling. The distributed properties of these FRBs are normalized and compared to the nine observed Hilat events.

[1] www.parkes.atnf.csiro.au/observing/documentation/user_guide

Slightly different selection criteria have been used by various authors to find FRBs. Thornton et al. (2013) used S/N>9 and DM>100 pc cm^{-3} and Champion et al. (2015) use the same selection criteria as Petroff et al. (2014), notably S/N$\geq$10, DM$\geq$ 0.9 $\times$ DM$_{\rm MW}$ and $W \leq$ 16.3 ms. We use the criteria S/N$\geq$10 and $W \leq$ 32.786 ms for the selection of the candidates in the simulations. We adopt an upper limit of 32.786 ms for the width motivated by the fact that the broadest FRB discovered in Hilat has a width of $\sim$19 ms, and in any case broader events still would have to be extremely bright to have S/N>10. We do not apply a DM threshold for the Hilat region as we are only sensitive to DM>100 pc cm^{-3} in keeping with Thornton et al. (2013), due to assuming the value of DM$_{\rm host}$ to be 100 pc cm^{-3}. Tests showed that the differences in these selection criteria are minor and have negligible effect on our basic results. In particular, every observed FRB fits each of these criteria.

3.1 Monte carlo results for Parkes

Figs 1 and 2 display the results of the simulations of the cosmic SFH ($\rho_{\rm FRB}(z) = \rho_{\rm SFH}(z)$) and constant-density ($\rho_{\rm FRB}(z) =$ constant) models with scattering included, as seen by Parkes, overlaid on histograms of the nine observed Hilat FRBs (Thornton et al. 2013; Champion et al. 2015). Fig. 1 shows observational parameters for each burst and Fig. 2 displays the parameters that are derived. We quantify the goodness of fit of the model to the observations in Section 3.2.

The fluence distribution of our simulated events is displayed in panel A of Fig. 1 and their S/N distribution in panel B, each compared to the nine Hilat events. All the observed Hilat FRBs have fluences between 0.7 and 7 Jy ms. Both models peak at $\sim$0.5 Jy ms and are reasonable matches to the observations. The S/N distributions of both models contain a large number of events just above the detection threshold of 10 and then gradually decline towards higher values; both appear to agree with the observations reasonably. Panel C shows the DM distribution of the models and the observations: this is similar to the panel showing the redshift distribution, since they are closely related. Both the cosmic SFH and constant density models are in agreement with the observed data.

The width of an FRB pulse affects its detection S/N. In the observer's rest frame, the width results from the sum of contributions from scattering due to the ISM and IGM (equations 4 and 5, see Bhat et al. 2004; Lorimer et al. 2013) DM smearing time and the intrinsic width. Panel D of Fig. 1 displays the distributions of the observed widths of the sources. We found neither model to agree with the data very well and may be a result of our simplistic model of intergalactic scattering discussed below.

The adopted model for the spatial density of the sources in Fig. 2 panel E does not have much effect on their redshift distribution, with only a small excess of sources produced at $0 < z < 0.5$ for the constant density model compared to the cosmic SFH model. As expected, we see a tendency for more events at higher redshift for the SFH model compared to the constant density model. Panel F shows the energy distribution (at source and in-band) of the FRBs and the models. Both models are only sensitive to the bright tail of the adopted lognormal energy distribution function and have similar mean values to that of the nine observed FRBs. Since the mean energy E_0 of the adopted luminosity function (LF) is a free parameter, we adjust this to achieve good fits to the observed luminosities in panel F of Fig. 1. Acceptable fits are obtained for both models by adopting $E_0 = 10^{31.2}$ J, with a lognormal scatter of $\sigma_{\rm logE} = 1.0$.

Table 2. K-S test results for the model distributions against data in Figs 1 and 2.

Parameter	p value	
	Cosmic SFH	Constant density
Redshift	0.543	0.048
Energy	0.884	0.186
Fluence	0.047	0.106
S/N	0.258	0.078
DM	0.730	0.053
Effective width	0.013	0.001

This adopted LF is a parametrized LF only and does not possess any physical significance.

3.2 Statistical analysis

Kolmogorov–Smirnov tests (K-S) were performed on all the distributions in Figs 1 and 2 and the resulting probability statistics p are given in Table 2. A p value of <0.05 is our criterion for deciding if the two distributions differ. Each model was compared against the data for the nine FRBs.

The p values show that both models are consistent with the observed distributions of redshift, energy, fluence S/N and DM but, as already noted above, we have difficulty modelling the effect of scattering on the FRBs. The p values of 0.013 (density of FRBs proportional to the cosmic SFH with redshift) and 0.001 (density of FRBs constant with redshift) reject the hypotheses that both models and the FRB data are from the same population. The present sample of nine events is thus insufficient to distinguish between these models per se (the poor match to the distribution of pulse widths in both models notwithstanding). For FRBs discovered at Parkes, our simulations indicate that of the order of 50 FRBs are required to distinguish between the two FRB number density models at the 95 per cent confidence level. This certainly highlights the need to discover FRBs more efficiently, as the present discovery rate is only of the order of 1 per 12 d on sky at Parkes.

To better understand the effective widths, the 14 FRBs at Parkes as a function of scattering time is shown in Fig. 3. The estimated widths of the events due to IGM scattering and a possible intrinsic width ($\tau_{\rm IGM}^2 + \tau_{\rm int}^2 = W^2 - \tau_{\rm DM}^2 - \tau_{\rm ISM}^2$ from equation 6) are plotted against our estimate of the contribution to the total DM due to the IGM alone ($\rm DM_{IGM} = DM_{tot} - DM_{ISM} - DM_{host}$ from equation 1). We see that the scattering times are inconsistent with equation (5), and show considerable scatter around it.

This result highlights the basic difficulty with the IGM model, apparent in the data (Fig. 3), that the pulse widths of the observed FRBs scatter around the adopted functional form for the IGM (equation 5). This behaviour is also seen for pulsars being scattered by the ISM, for which there is at least an order of magnitude scatter in the data around the observed pulse width trend (equation 4; see Bhat et al. 2004). If we assume that there is a similar scatter around $\tau_{\rm IGM}$ of an order of magnitude, we still do not acquire satisfactory fits to the data within 2σ confidence. This suggests that the scattering is not due to a line-of-sight dependent inhomogeneous IGM. It may be due to interaction with the ISM of an intervening galaxy or an intracluster medium along the line of sight, although the probability of intersection at the redshifts modelled is quite low and only a small fraction of lines of sight may be affected (Macquart & Koay 2013). We have not attempted to model such effects: our aim is to test a much simpler model before adding in difficult to test assumptions about the properties of the IGM.

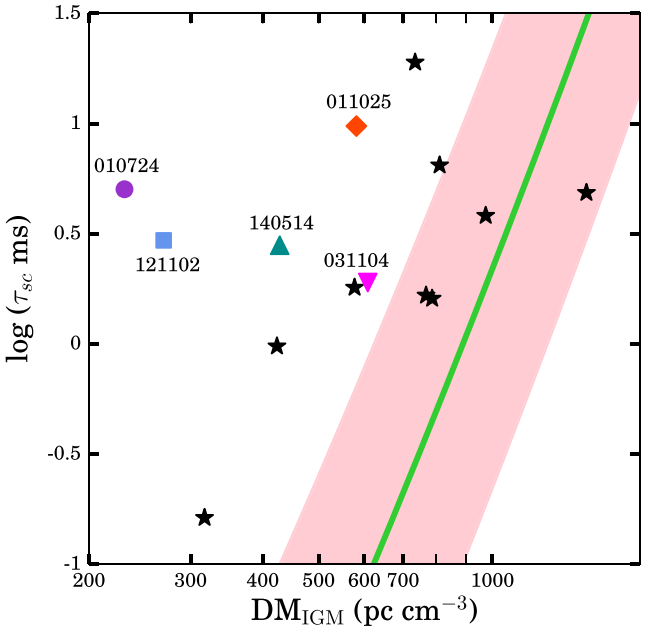

Figure 3. Adopted model of the scattering time due to the IGM (solid) at 1.4 GHz for Parkes versus estimated DMs. Stars represent the nine Hilat events and other markers represent FRBs discovered in various other surveys. The shaded region around the fitted line to the equation represents the order of magnitude scatter adopted in the simulation. Note that one Hilat FRB lies below the IGM scattering relation (see equation 5) but is still within the adopted 1σ spread.

If we assume that our simulated events have a mean intrinsic width of 3 ms (with a standard deviation of 3 ms, truncated at 0 ms), the resulting width distributions are found to be in good agreement with the observed nine Hilat FRBs. The intrinsic width assumption is motivated by FRB121002 and FRB130729 (Champion et al. 2015) which have hints of double, rather than single peaked pulse profiles. This is a rather ad hoc assumption and further work on this is required once the population is expanded. The disagreement of the distribution of event widths with the observations is the weakest point in our modelling. Clearly, there is a need for more FRBs to resolve this problem.

3.3 The log$N$–log$\mathcal{F}$ of the Hilat events

In a Euclidean Universe populated with events (or objects) of fixed luminosity (i.e. standard candles) and uniform number density, the number N detected above some flux limit S varies as $N \propto S^{\alpha}$, where $\alpha = -3/2$. In our model, the FRBs have a very broad luminosity distribution and are sufficiently distant that non-Euclidean effects are important. Consequently, we do not expect to see $\alpha = -3/2$.

The very wide range of luminosities of the observed events suggests they are not particularly good standard candles, and until we have a redshift of an FRB host galaxy, or some other independent distance indicator for an FRB, their luminosities are highly dependent on the assumption that DM is a proxy for redshift. The luminosities are dependent on each line of sight being equal to the average line of sight in a ΛCDM Universe. In fact, it is the small deviations from this that we will use to do some cosmology, when we have a lot of FRBs with real redshifts. In any case, our FRB simulations are for a ΛCDM cosmology, which affects α. In a ΛCDM cosmology, α varies smoothly from a slope of $-3/2$ for the nearby universe, gradually becoming flatter as further distances are probed.

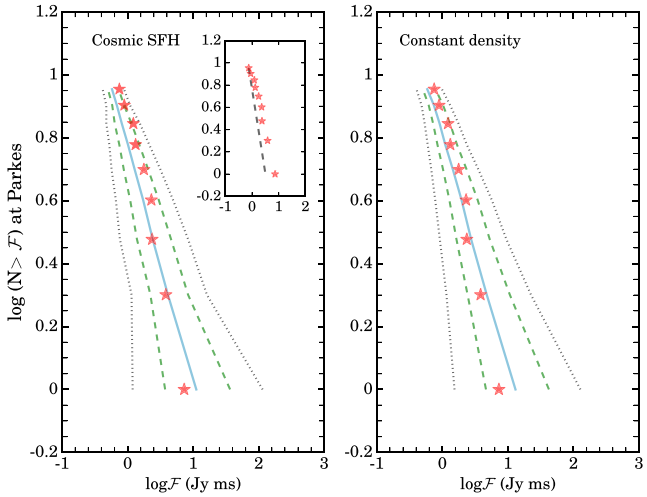

Figure 4. The log$N$–log$\mathcal{F}$ curves for the nine Hilat FRBs and the simulation samples. The left-hand panel displays the cosmic SFH (Hopkins & Beacom 2006) scenario and the right-hand panel displays the constant density scenario. Stars represent the nine Hilat FRBs and the solid line connects the medians of the number densities as a function of fluence for the simulation sample. The dashed and dotted lines represents the 1σ and 2σ limits around the median for each N. The inset in the left-hand panel exhibits the nine observed FRBs and a fitted slope of $\alpha = -3/2$ for comparison.

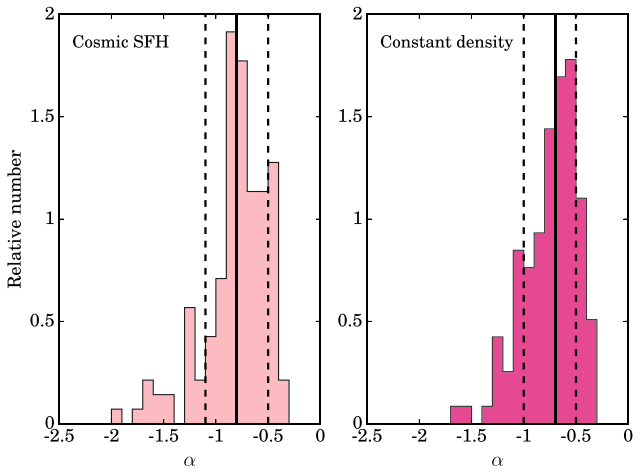

Figure 5. The histograms display the slopes α, of the simulation samples containing exactly nine events each. The left-hand panel represents the cosmic SFH scenario and the right-hand panel represents the constant density scenario. The medians of the histograms are represented by the solid lines and the 1σ scatter from the median is marked by the dashed lines. The slope of the nine FRBs $\alpha = -0.9 \pm 0.3$ is found to be consistent with the simulations within the uncertainties.

To illustrate, at a redshift of $z \sim 0.7$, typical of FRBs found to date, standard candles yield a relation with a slope of $\alpha \sim -1$. There are additional factors which affect α. First, the HTRU survey is 'fluence incomplete' in the sense that events with the same fluence are easier to detect if they have narrower pulse widths. Secondly, propagation of FRB pulses through the IGM causes the pulses to broaden, reducing their S/N, so that an S/N selected sample effectively has a distance horizon beyond which pulses are too scattered to see. This will flatten the relation as we probe to dimmer events.

It is possible to select a 'fluence complete' sample of the FRBs, and compare these to simulation events selected in the same way, but this would reduce our sample of nine events to just four events. For an S/N of 10, the fluence completeness limit for Hilat is ∼2 Jy ms (Keane & Petroff 2015). This is an observational selection, and affects the slope α, of the relation. It is straightforward to include this effect in the simulations, however, due to our already small sample of events we prefer to compare to the full set of nine events selected by S/N, rather than a fluence complete set of four events.

The log$N$–log$\mathcal{F}$ plot of the nine Hilat events is shown in Fig. 4 – note that we use the fluence $\mathcal{F}$ in Jy ms (since FRB detections are width dependent) for what would normally be flux density S in Jy. The cumulative log$N$–log$\mathcal{F}$ relation is reasonably linear for the nine events, and has a slope of $\alpha = -0.9 \pm 0.3$. For the cumulative curve of only nine events, sample variance is likely to be a significant factor. We use the simulations of Hilat (as described in Section 2 with selection criteria described in Section 3), which were set up to yield of the order of nine events per run to estimate the error on α. Those realizations which had exactly nine events were used for comparison with the nine observed Hilat events. We have fitted slopes (α) to these simulated nine event samples and show the distribution of α in Fig. 5. The typical error on α is ± 0.1 which is the adopted bin size in Fig. 5. The median slope obtained is $\alpha = -0.8$ for the SFH case and $\alpha = -0.7$ for the constant density case, but with significant scatters (the 1σ limits are shown as dashed lines) of the order of ± 0.3 for the SFH and ± 0.2 for the constant density around the mean. Our observed slope of $\alpha = -0.9 \pm 0.3$ is consistent with both models.

We conclude that the slope of the log$N$–log$\mathcal{F}$ relation of the nine observed events is consistent to within the uncertainties of both the simulated models, indicating that our measured log$N$–log$\mathcal{F}$ slope is consistent with FRBs being of cosmological origin. This is in agreement with the conclusion of Katz (2015) that the log$N$–log$S$ and N versus DM distributions are consistent (except for the anomalously bright Lorimer burst) with cosmological distances inferred from their DM in a simple approximation to standard cosmology.

3.4 Medlat versus Hilat

The Medlat component of the HTRU survey consists of 540 s pointings in the range $-120^\circ < l < 30^\circ$ and $|b| < 15^\circ$. Petroff et al. (2014) found no FRBs in this region of the survey. Under the assumption that FRBs are isotropically distributed, scaling from Hilat, and accounting for a slight reduction in their detectable source density in the Medlat region due to the smearing effects of the ISM, they estimate the probability of this occurring by chance as only of the order of 0.5 per cent. We simulate both the Medlat and Hilat regions (adopting 100 per cent of Hilat and 100 per cent of Medlat as the surveyed completeness for the regions for FRBs) to determine the likelihood of finding zero FRBs in Medlat for nine discovered FRBs in Hilat. The simulation for Medlat is otherwise identical to the one described in Section 2 except for the survey parameters, i.e. number of pointings, region of sky surveyed, $T_{\rm sky}$ corresponding to the region of sky surveyed and integration time per pointing. The same selection criteria as described in Section 3 are used for selection of candidates in both Medlat and Hilat.

We obtain an average of $\sim 3 \pm 2$ events in our Medlat simulations for every nine events in the Hilat simulations, finding no events just 5.1 per cent of the time (Fig. 6). The estimated probability of zero events being seen in Medlat 0.5 per cent of the time made by Petroff et al. (2014) is based on the four events detected in the 24 per cent of the Hilat survey which had been searched at the time. The higher probability we estimate of finding no events in Medlat

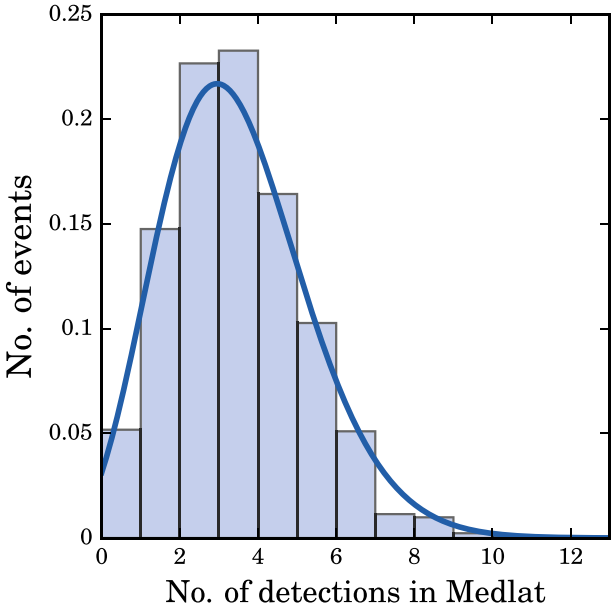

Figure 6. Number of FRBs expected in Medlat normalized to the nine events in Hilat. Both surveys are assumed to be fully searched for FRBs. The histogram represents the number of FRBs expected in Medlat for a corresponding nine FRBs detected in Hilat. A Poissonian curve is fitted to the data. The number of FRBs found in Medlat is zero 5.1 per cent of the time.

in our simulations is due to our using the lower all sky rate, now that Hilat has been completely searched and it only yielded nine FRBs.

4 THE LOGN–LOG$\mathcal{F}$ OF FRB EVENTS

Our simulations have been used to generate FRB events at two facilities – Parkes and UTMOST (Bailes et al. in preparation). UTMOST is the recently upgraded Molonglo Observatory Synthesis Telescope located about 300 km south-west of Sydney, near Canberra, and is a field station of the University of Sydney. We generate events for the specifications of UTMOST and Parkes for the soon to be installed phased array feed (PAF) receiver in comparison with the current MB receiver at Parkes. The FRB comoving density models, and energy distributions are the same as those described in Section 2. The effective pulse width of each event is computed using equation (6). The S/N of the events were reduced by a factor of 4 for the events at UTMOST to account for the fact that it is less sensitive than the MB receiver at Parkes (Caleb et al. 2016). The Parkes PAF is estimated to have ∼50 per cent of the sensitivity of the MB[2] which is accounted likewise. The S/Ns at both telescopes were further reduced by $\sqrt{W}$ before making the cut-off of S/N≥10 and $W \leq 32.786$ ms.

Fig. 7 shows the cumulative log$N$–log$\mathcal{F}$ curves at UTMOST and at Parkes for both the MB and PAF. These curves do not include the effects of fluence completeness. All curves have been normalized to their respective FRB rates in Table 3, which have been calculated assuming a Euclidean Universe where the cumulative number density scales as $\propto \mathcal{F}^{\alpha}$ where $\alpha = -3/2$ (Caleb et al. 2016). This is a conservative option, as the slope of this relation is most likely flatter

[2] http://www.atnf.csiro.au/management/atuc/2013dec/science_meeting/ATUC_PKS_receivers.pdf

Table 3. Minimum detectable flux density for a 10σ, 1 ms event and event rate assuming a Euclidean scaling for the Parkes MB, Parkes PAF and UTMOST

Telescope/Receiver	$S_{\rm min}$ (Jy)	Rate (events d^{-1})
Parkes MB	0.4	0.08±0.03
Parkes PAF	0.6	0.10±0.04
UTMOST	1.6	0.16±0.06

(as seen in the previous section), and underestimates the number of events expected.

5 DISCUSSION AND CONCLUSIONS

We have simulated observational and derived properties of a cosmologically distributed population of FRBs, for comparison with the nine FRBs seen in the HTRU/Hilat survey conducted at Parkes from 2008 to 2014. Two models for the spatial number density of the FRBs are examined: first, where the comoving density is a constant, and secondly, where the number of FRBs is proportional to the cosmic SFH. The properties of the ISM in the Milky Way and a putative host galaxy for the FRB are taken into account, and conservative assumptions are made about the properties of the IGM, the spectral index of FRBs and their LF.

The simulated distributions of redshift, energy, DM, S/N, fluence and effective widths for both the cosmic SFH and constant density models were compared to the nine observed FRBs. We achieved reasonable matches to the data for all these properties except the event widths, by adjusting only the typical FRB event energy at source (and scatter around this energy), i.e. by adjusting only their LF. It proved difficult to fit the distribution of FRB widths without making ad hoc assumptions about scattering in the IGM or the intrinsic widths of the pulses. The simulations are intended to look at FRB properties with as simple an assumption set as possible; adding in poorly constrained properties as these for the FRBs and the IGM for the sake of fitting the pulse widths was not pursued. As the pulse widths probe completely different properties of FRBs and the IGM, this may prove more fruitful to understanding their origin as more FRBs are found.

The most interesting property of the simulated events is their distribution of log$N$–log$\mathcal{F}$, where N is the number of events detected above some fluence $\mathcal{F}$. If the sources have an even approximately typical luminosity (i.e. are standard candle-like) then the slope of this relation is a probe of their spatial distribution. For standard candles of flux S distributed uniformly in empty, Euclidean space, the slope of the closely related log$N$–log$S$ relation is well known to be exactly $-3/2$. For FRBs, the slope of the relation is affected substantially for three main factors: first by cosmology (space is non-Euclidean); secondly by propagation through the IGM (i.e. space is not empty) and thirdly by selection effects at the telescope (narrower events are detected more readily than broader ones). A major aim of the simulation is to quantify these effects.

The observed slope α of the log$N$–log$\mathcal{F}$ of the nine FRBs analysed is $\alpha = -0.9 \pm 0.3$. Our simulations are able, in both scenarios for the number density of the sources with redshift, to match this slope well, yielding $\alpha = -0.8 \pm 0.3$ for the cosmic SFH and $\alpha = -0.7 \pm 0.2$ for the constant density case. We conclude that the properties of the observed FRBs are consistent with arising from sources at cosmological distances, with the important caveat that the pulse width distribution does not match our simulation results particularly well.

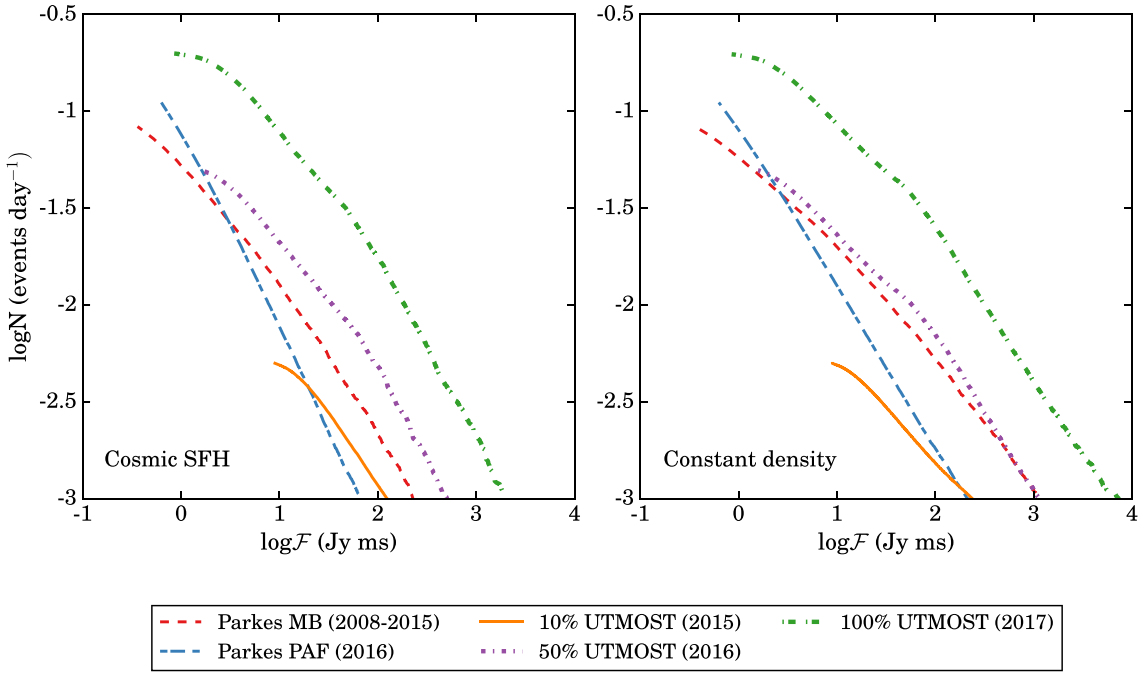

Figure 7. The log$N$–log$\mathcal{F}$ curves for different fractional sensitivities at UTMOST and MB and PAF receivers at Parkes. The left-hand panel displays the log$N$–log$\mathcal{F}$ curves for the cosmic SFH (Hopkins & Beacom 2006) model of the FRB space density with redshift and the right-hand panel displays the curves for the constant density model. All curves include the ISM and IGM scattering and are normalized to the rate of $\sim$ 1 event per 12 d at the Parkes MB and additionally to the ratio of their fields of view for UTMOST and the Parkes PAF. Uncertainty in the PAF design sensitivity makes prediction difficult, but its wider sky coverage can increase the Parkes discovery rate at lower fluences. The fully sensitive UTMOST will dominate the event detection rate at all fluences.

The LF of the FRBs is the main free parameter in the simulations. We adopt a lognormal LF and adjust the mean energy E_0 and spread in energy $\sigma_{\log E}$. It is clear from the nine observed events that a narrow, standard candle-like LF is an unacceptable fit, since their inferred intrinsic luminosities have a spread of about an order of magnitude. We measure a mean energy E_0 of $\sim 10^{31.2}$ J with a spread of a factor of 10 in energy. As the observed FRBs very much sample only the high-luminosity tail of this distribution, other choices for the LF, such as a truncated power law would also adequately match the data. Our studies show that the beam pattern of the telescope has a strong effect only when the number of FRBs is large ($\gtrsim$ few $\times$ 100), which is then sensitive to the high-luminosity tail of events. The LF choice affects the distributions strongly even for small samples: an LF with a significant spread in luminosity is required to model the nine events. Finally, our simulations show that the adopted comoving density models for the FRBs has weak effects, and large sample sizes ($\gtrsim$ 100) are required to probe this.

Future work could implement other LF choices and investigate the extent to which the LF and SFH and beam pattern affect the observed distributions analysed in this paper: the small number of FRBs detected to date do not warrant such work here.

Our simulations show that at least 50 FRB events are required to distinguish, at the 95 per cent confidence level, between our two tested models for their cosmological spatial distributions for the specifications of the Parkes telescope. This argues strongly for projects to increase the detection rate of FRBs by using wide field-of-view instruments, such as UTMOST and CHIME (Bandura et al. 2014). Even more important in the immediate future is to localize events on the sky (to find putative host galaxies for FRBs) and a number of experiments are ongoing to do this (e.g. SUPERB project at Parkes).

We have applied our simulations to the Medlat survey at Parkes (which is part of the HTRU survey), which surveyed a lower Galactic latitude region of the sky with longer integrations. Our simulations of this survey supports the conclusion of Petroff et al. (2014) that the sky rate of FRBs in Thornton et al. (2013) is overestimated by about 50 per cent, or that FRBs are not distributed isotropically on the sky.

We simulate FRB rates at two other facilities: at UTMOST (first survey results of which are in a companion paper Caleb et al. 2016) and at Parkes with the planned PAF, under conservative assumptions about the spectral index of FRBs, and the sensitivity of the instruments. UTMOST has the capability, at full design sensitivity to dominate the FRB detection rate. Uncertainty in the final PAF design sensitivity makes prediction difficult, but its wide sky coverage has the potential to increase the FRB discovery rate of FRBs close to the fluence limit. The fully sensitive UTMOST will dominate the event detection rate at all fluences.

ACKNOWLEDGEMENTS

The authors gratefully acknowledge valuable discussions with E. Petroff, J.P. Macquart and Alan R. Duffy. This work used the gSTAR national facility which is funded by Swinburne and the Australian Governments Education Investment Fund. Parts of this research were conducted by the Australian Research Council Centre for All-Sky Astrophysics (CAASTRO), through project number CE110001020.

REFERENCES

Bandura K., Addison G. E., Amiri M., Bond J. R., Campbell-Wilson D., Connor L., Cliche, 2014, in Stepp L. M., Gilmozzi R., Hall H. J., eds, Proc. SPIE Conf. Ser. Vol. 9145, Ground-based and Airborne Telescopes V. SPIE, Bellingham, p. 914522

Bhat N. D. R., Cordes J. M., Camilo F., Nice D. J., Lorimer D. R., 2004, ApJ, 605, 759
Burke-Spolaor S., Bannister K. W., 2014, ApJ, 792, 19
Burke-Spolaor S., Bailes M., Ekers R., Macquart J.-P., Crawford F., III, 2011, ApJ, 727, 18
Champion D. J., Petroff E., Kramer M., Keith M. J., Bailes M., Barr E. D., Bates S. D., Bhat N. D. R., 2015, preprint (arXiv:1511.07746)
Caleb M. et al., 2016, preprint (arXiv:1601.02444)
Connor L., Sievers J., Pen U.-L., 2015, preprint (arXiv:1505.05535)
Cordes J. M., Lazio T. J. W., 2002, preprint (astro-ph/0207156)
Cordes J. M., McLaughlin M. A., 2003, ApJ, 596, 1142
Cordes J. M., Wasserman I., 2016, MNRAS, 457, 232
Falcke H., Rezzolla L., 2014, A&A, 562, A137
Fukugita M., Peebles P. J. E., 2004, ApJ, 616, 643
Fuller J., Ott C. D., 2015, MNRAS, 450, L71
Haslam C. G. T., Salter C. J., Stoffel H., Wilson W. E., 1982, A&AS, 47, 1
Hassall T. E., Keane E. F., Fender R. P., 2013, MNRAS, 436, 371
Hopkins A. M., Beacom J. F., 2006, ApJ, 651, 142
Inoue S., 2004, MNRAS, 348, 999
Ioka K., 2003, ApJ, 598, L79
Kashiyama K., Ioka K., Mesaros P., 2013, ApJ, 776, L39
Katz J. I., 2014, Phys. Rev. D, 89, 103009
Katz J. I., 2015, preprint (arXiv:1505.06220)
Keane E. F., Petroff E., 2015, MNRAS, 447, 2852
Keane E. F., Stappers B. W., Kramer M., Lyne A. G., 2012, MNRAS, 425, L71
Keith M. J. et al., 2010, MNRAS, 409, 619
Kulkarni S. R., Ofek E. O., Neill J. D., Zheng Z., Juric M., 2014, ApJ, 797, 70
Loeb A., Shvartzvald Y., Maoz D., 2014, MNRAS, 439, L46
Lorimer D. R., Bailes M., McLaughlin M. A., Narkevic D. J., Crawford F., 2007, Science, 318, 777
Lorimer D. R., Karastergiou A., McLaughlin M. A., Johnston S., 2013, MNRAS, 436, L5
Luan J., Goldreich P., 2014, ApJ, 785, L26
Lyubarsky Y., 2014, MNRAS, 442, L9
Macquart J.-P., Koay J. Y., 2013, ApJ, 776, 125
Masui K. et al., 2015, Nature, 528, 523
Mottez F., Zarka P., 2014, A&A, 569, A86
Petroff E., van Straten W., Johnston S., Bailes M., Barr E. D., Bates S. D., 2014, ApJ, 789, L26
Petroff E., Bailes M., Barr E. D., Barsdell B. R., Bhat N. D. R., Bian F., Burke-Spolaor S., Caleb M., 2015a, MNRAS, 447, 246
Petroff E., Keane E. F., Barr E. D., Reynolds J. E., Sarkissian J., Edwards P. G., Stevens J., Brem C., 2015b, MNRAS, 451, 3933
Popov S. B., Postnov K. A., 2013, preprint (arXiv:1307.4924)
Ravi V., Shannon R. M., Jameson A., 2015, ApJ, 799, L5
Reich P., Reich W., 1988, A&AS, 74, 7
Robles J. A., Lineweaver C. H., Grether D., Flynn C., Egan C. A., Pracy M. B., Holmberg J., Gardner E., 2008, ApJ, 684, 691
Savage B. D., Kim T.-S., Wakker B. P., Keeney B., Shull J. M., Stocke J. T., Green J. C., 2014, ApJS, 212, 8
Spitler L. G. et al., 2014, ApJ, 790, 101
Thornton D., Stappers B., Bailes M., Barsdell B., Bates S., Bhat, 2013, Science, 341, 53
Totani T., 2013, PASJ, 65, L12
Wright E. L., 2006, PASP, 118, 1711
Xu J., Han J. L., 2015, Res. Astron. Astrophys., 15, 1629

This paper has been typeset from a TEX/LATEX file prepared by the author.